RSC Advances

PAPER

View Article Online
View Journal | View Issue

Cite this: *RSC Adv.*, 2024, **14**, 1207

Paper-based ratiometric fluorescent sensing platform based on mixed quantum dots for the detection of glucose in urine

Keke Song, Chenying Liu, Guangbin Chen, Wenhao Zhao, Shufang Tian and Qian Zhou *

A paper-based ratiometric fluorescent sensing platform has been developed for glucose detection based on a dual-emission fluorescent probe consisting of carbon quantum dots (C QDs) and CdTe QDs. When the two kinds of QDs are mixed, the fluorescence of C QDs is reversibly quenched by CdTe QDs. However, in the presence of glucose, the fluorescence of CdTe QDs is quenched by H_2O_2 catalyzed by glucose oxidase (GOx), which restores the fluorescence of C QDs. The proposed paper-based ratiometric fluorescent sensing platform exhibited good sensitivity and selectivity towards glucose. The working linear range was 0.1 mM to 50 mM with a limit of detection (LOD) of 0.026 mM. Additionally, the proposed paper-based sensor possesses viability for the determination of glucose in actual urine samples.

Received 18th October 2023
Accepted 18th December 2023

DOI: 10.1039/d3ra07082d

rsc.li/rsc-advances

1. Introduction

Glucose plays a crucial role in life processes as the main energy source and metabolic intermediate.[1,2] Chronically high levels of glucose in the body can cause many endocrine metabolic diseases, such as diabetes.[3] As a chronic disease, diabetes often leads to many comorbidities, including retinopathy, blindness, heart disease, kidney failure, and strokes.[4–7] Studies on diabetes management have shown that strict sugar control to maintain glucose levels in a normal range can delay the onset and progression of complications related to diabetes and improve the survival of diabetes patients.[8–10] Constant glucose monitoring is essential for people with diabetes, usually *via* an invasive process (puncturing a finger 5–10 times a day) to achieve glucose analysis in blood.[11,12] Although it is common to monitor blood glucose, repeated pinpricks could bring patients pain, anxiety and even infection risk. Recently, alternative noninvasive and painless methods have been developed by changing the sampling target from blood to other body fluids such as tears,[13] saliva,[14] urine[15] and sweat.[16] It should be noted that elevated glucose levels in urine do not necessarily mean diabetes. In the case of renal glycosuria, the glucose levels in urine are elevated while the blood glucose remains normal.[17] Despite this, it is generally believed that glucose level in urine is proportional to blood in the case of the diabetic.[18,19] Thus, developing noninvasive tools to achieve reliable and convenient monitoring of glucose in urine has significant value to offer.

To date, various methods have been applied for glucose analysis, such as electrochemistry,[20] colorimetry,[21] chemiluminescence,[22] fluorimetry,[23] and surface-enhanced Raman spectroscopy.[24] Among them, fluorescent techniques have attracted much attention due to their high sensitivity, visual detection, simplicity, fast response and low cost. A variety of fluorescent materials, including organic dyes,[25] noble metal (gold, silver, copper) nanoclusters,[26–28] carbon quantum dots,[29] semiconductor quantum dots,[30] have shown great potential in the fluorescent sensing field. However, most traditional fluorescent sensing systems are based on a single emission signal, which has been susceptible to a number of analyte-independent factors such as instrumental deviation, environmental fluctuations, local concentration variance of probes and the sample matrix.[31,32] To avoid such situations, the design of fluorescent sensing systems has adopted a ratiometric approach by introducing two or more fluorescent signals. The ratiometric fluorescent sensor monitors emission intensities at two or more wavelengths simultaneously, and the intensity ratios are calculated and calibrated for analyte quantification. Compared with single emission sensing mode, the ratiometric fluorescent sensor provides built-in correction, leading to minimized interference, improved signal-to-noise ratios and enhanced analytical accuracy.[33,34] Moreover, multicolor variations of the fluorescent signal could be observed during the sensing process, which is conducive to direct visual discrimination with the naked eye.

With the increasing need and development of point-of-care testing, paper-based analytical devices have been developed and attracted a great deal of research due to their multiple advantages, including small sample volume, low cost, simple

Henan International Joint Laboratory of Medicinal Plants Utilization, College of Chemistry and Molecular Sciences, Henan University, Kaifeng 475000, China

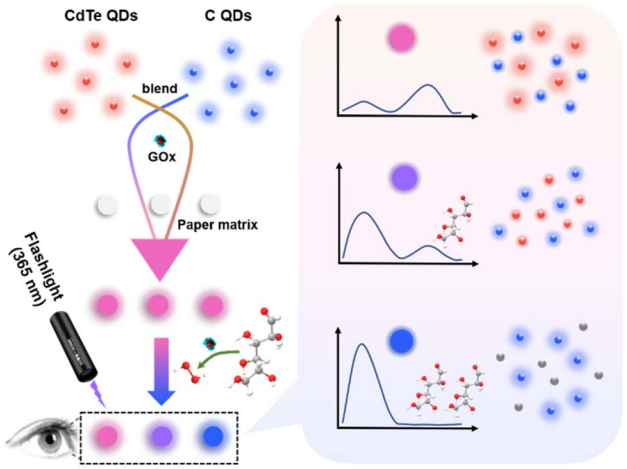

Scheme 1 Schematic illustration of the paper-based ratiometric fluorescent sensing platform for glucose detection.

fabrication, ultimate portability and rapid assay.[35–37] Paper is a promising substrate for constructing sensing platforms since it is cheap, disposable, biocompatible, stable and easy to modify. Herein, a paper-based ratiometric fluorescent sensing platform was successfully fabricated for the analysis of glucose in urine (Scheme 1). Carbon quantum dots (C QDs) with blue emission and CdTe quantum dots (CdTe QDs) with red emission were synthesized and mixed at a proper ratio to achieve dual-emission. Then, the paper-based ratiometric fluorescent sensing platform could be obtained by modifying the paper with the mixture of quantum dots and glucose oxidase (GOx). The target glucose could be catalyzed by GOx to produce hydrogen peroxide (H_2O_2), which could subsequently quench the fluorescence of CdTe QDs and result in the recovery of C QDs fluorescence. With the increasing concentration of glucose, the fluorescence of CdTe QDs decreased while the fluorescence of C QDs increased. A good linear relationship between the intensity ratios and glucose concentrations could be obtained. Moreover, multiple color changes of the fluorescent signal could be observed with the naked eye during the sensing process under a 365 nm UV lamp, which is conducive to direct visual discrimination.

2. Experimental section

2.1 Materials and reagents

Tris(hydroxymethyl)aminomethane (Tris), sodium hydroxide (NaOH), sodium tellurite (Na_2TeO_3), potassium borohydride (KBH_4), urea (H_2NCONH_2), isopropyl alcohol (C_3H_8O), sodium phosphate dibasic (Na_2HPO_4) were purchased from Shanghai Aladdin Biochemical Technology Co., Ltd. (Shanghai, China). Citric acid monohydrate ($C_6H_8O_7 \cdot H_2O$), fructose and α-lactose monohydrate were purchased from Beijing InnoChem Science & Technology Co., Ltd. (Beijing, China). Sodium phosphate monobasic (NaH_2PO_4) and 3-mercaptopropionic acid (MPA) were purchased from Sigma-Aldrich. Cadmium nitrate tetrahydrate ($Cd(NO_3)_2 \cdot 4H_2O$), trisodium citrate dihydrate ($C_6H_5Na_3O_7 \cdot 2H_2O$), D(+)-glucose monohydrate ($C_6H_{12}O_6 \cdot H_2O$), maltose ($C_{12}H_{22}O_{11}$), sucrose ($C_{12}H_{22}O_{11}$) were purchased from Sinopharm Chemical Reagent Co., Ltd. (Shanghai, China). Glucose oxidase (GOx) and fetal bovine serum were purchased from Sangon Biotech Co., Ltd. (Shanghai China). Hydrogen peroxide (H_2O_2, 30% w/w) was purchased from Haohua Chemical Reagent Co., Ltd. (Luoyang, China). All other reagents were used as received without further purification. All aqueous solutions in this work were prepared by using ultrapure water from a Millipore ultrapure water system (18.2 MΩ cm at 25 °C, Milli-Q).

2.2 Apparatus

Transmission electron microscopy (TEM) measurements were performed on a JEM-F200 (200 kV) (JEOL, Japan). Powder X-ray diffraction (XRD) patterns were measured by a D8 Advance X-ray powder diffractometer (Bruker, Germany). Fluorescence spectra were recorded using an F-7000 fluorescence spectrophotometer (Hitachi, Japan). Visual fluorescent colors were collected with a smartphone after excitation with a 365 nm UV lamp.

2.3 Synthesis of MPA-modified CdTe QDs

The water-soluble MPA-modified CdTe QDs were synthesized according to the literature with slight modification.[38,39] Initially, 118 mg of $Cd(NO_3)_2 \cdot 4H_2O$ and 200 mg of trisodium citrate dihydrate were added to 50 mL of ultrapure water under ultrasonic condition to produce a clear solution, followed by the addition of MPA (55 μL). Then, the pH of the resulting mixture was adjusted to 10.5 using 1.0 M NaOH aqueous solution. Subsequently, 22.2 mg of Na_2TeO_3 and 50 mg of KBH_4 were added into the mix and refluxed for 120 min. The obtained suspension was allowed to cool at room temperature and precipitated with isopropyl alcohol. Finally, the MPA-capped CdTe QDs were washed three times with isopropyl alcohol and dried overnight in a vacuum at 70 °C.

2.4 Synthesis of C QDs

The carbon quantum dots (C QDs) were synthesized by a one-step hydrothermal method.[40] Firstly, 1.0543 g of citric acid monohydrate and 0.6090 g of Tris were dissolved in 10 mL of ultrapure water under ultrasonic condition to produce a clear solution. Then, the solution was transferred into a Teflon-lined autoclave (25 mL) and heated at 200 °C for 6 h. Finally, the obtained C QDs solution was filtered by 0.22 μm filter membrane and stored at 4 °C for further use.

2.5 Fabrication of the paper-based fluorescent sensing platform

The paper-based fluorescent sensing platform was constructed through the co-immobilization of QDs and GOx on paper.[41] Prior to fabrication, chromatography paper (3.0 MM CHR, 20 × 20 cm, cat. no. 3030-861, Whatman, U.K.) was cut into a number of circular paper sheets with a diameter of 6.0 mm by using a Deli perforator (no. 0104, Zhejiang, China). Subsequently, 250 μL of C QDs solution, 250 μL of CdTe QDs solution (1 mg mL^{-1})

and 100 μL of GOx solution (40 U mL^{-1}) were mixed well to achieve a uniform suspension for preparation of the multi-functional paper-based sensing platform. Then, the circular paper was immersed into the above-prepared QDs-GOx homogeneous suspension and gently shaken at room temperature for 60 min. Finally, the circular paper was taken out and dried at 37 °C. For the sake of good reproducibility and precision, the obtained paper-based sensor was stored in a refrigerator at 4 °C for subsequent use.

2.6 Ratiometric fluorescent detection of glucose

Typically, 10 μL of glucose aqueous solutions with varying concentrations, ranging from 0.0 to 50 mM, were added to the prepared paper-based sensors. After allowing them to react at room temperature for 50 minutes, changes in the fluorescent color of the circular paper-based sensors were observed under a 365 nm UV lamp. The fluorescence spectra were also recorded using an F7000 fluorescence spectrophotometer by exciting the samples with a single wavelength at 365 nm.

2.7 Real samples assay

Urine samples used in this work were obtained from three healthy volunteers between the ages of 25 and 27. For glucose detection, all the urine samples were diluted with an equal volume of phosphate buffer solution (PBS) (0.1 M, pH 7.0). Then, standard glucose aqueous solutions were added to prepare the spiked samples. Eventually, 10 μL of the spiked urine samples were determined using the paper-based ratiometric fluorescent sensors. The fluorescent color of QDs-GOx paper sensors was observed under a 365 nm UV lamp and photographed by a smartphone. The fluorescent spectra were collected by an F7000 fluorescence spectrophotometer.

3. Results and discussions

3.1 Characterization of C QDs and CdTe QDs

Transmission Electron Microscope (TEM) was applied to investigate the morphological characteristics of C QDs and CdTe QDs. Fig. 1A shows the obtained C QDs with good dispersion and particle sizes of 2–6 nm. High-resolution transmission electron microscopy (HR-TEM) image of the C QDs (inset in Fig. 1A) reveals the lattice spacing of C QDs (~0.28 nm), which is close to the (100) facet of graphitic carbon.[42–44] The relatively uniform distribution of CdTe QDs with sizes of 2–5 nm could be seen from Fig. 1B. HRTEM image (inset in Fig. 1B) shows good crystalline structure of CdTe QDs and the lattice spacing (~0.36 nm) is consistent with (111) facet of CdTe QDs.[45] Moreover, XRD patterns of the prepared C QDs and CdTe QDs are displayed in Fig. 1C. A broad peak at about 23.4° assigning to the (002) of the graphitic carbon[42–44] and three obvious diffraction peaks at 25.2°, 43.1° and 49° corresponding to the (111), (220) and (311) of CdTe[46] could be observed. Fluorescence spectra of the C QDs and CdTe QDs were recorded

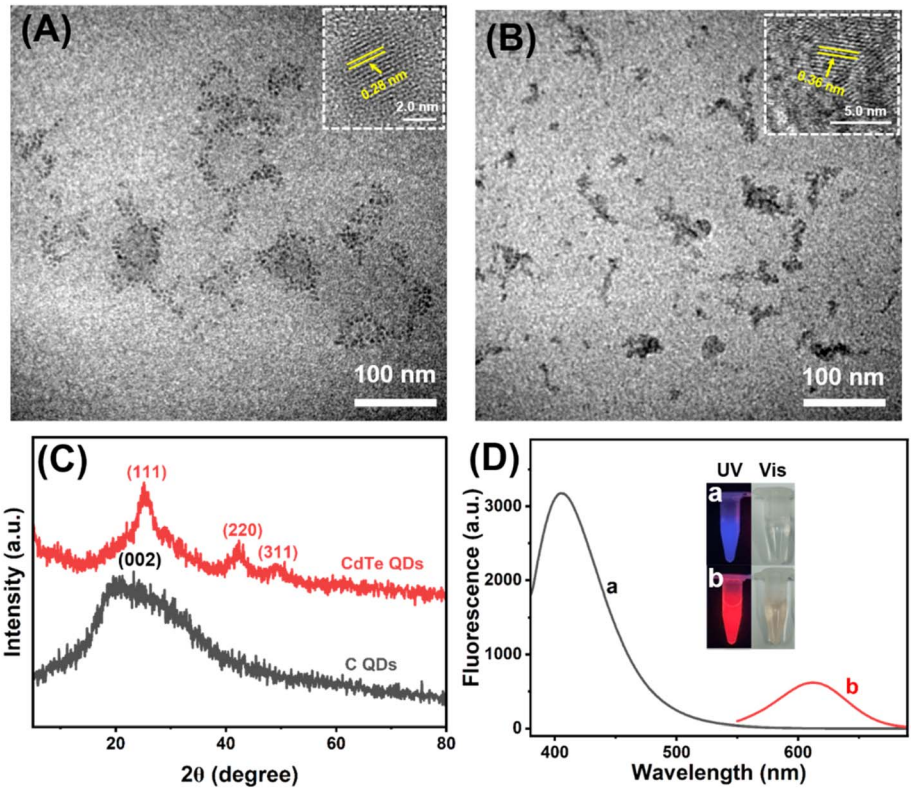

Fig. 1 TEM images and HR-TEM images (inset) of (A) C QDs and (B) CdTe QDs. (C) XRD spectrum of the C QDs and CdTe QDs. (D) Fluorescence spectra of C QDs (a) and CdTe QDs (b), Insets show the photographs of corresponding solutions under a 365 nm UV lamp (left) and day light (right) irradiation.

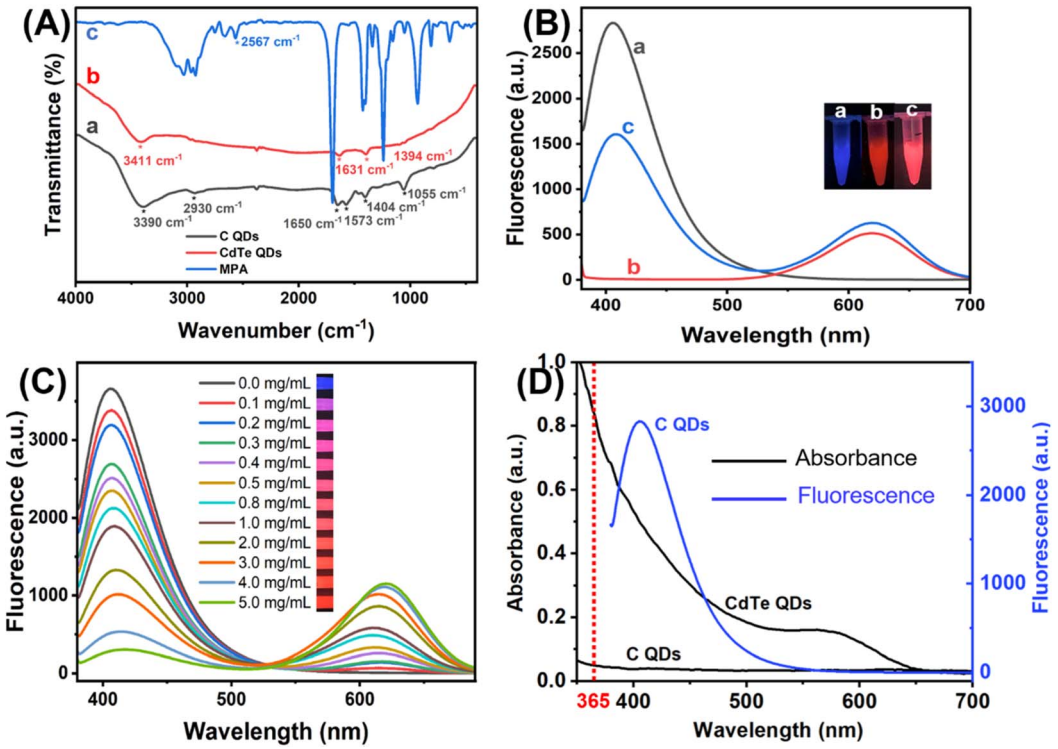

Fig. 2 (A) FT-IR spectra of C QDs (a), CdTe QDs (b) and MPA (c). (B) Fluorescence spectra of C QDs (a), CdTe QDs (b) and the mixture of C QDs and CdTe QDs (c) at the excitation of 365 nm (the inset photos were taken under a 365 nm UV lamp). (C) Fluorescence spectra of mixed QDs with different concentration of CdTe QDs (from 0.0 to 5.0 mg mL^{-1}). (D) UV-vis absorption spectra of the QDs and fluorescence spectrum of C QDs excited by a 365 nm UV light.

at 365 nm excitation wavelength. As seen from Fig. 1D, the maximum emission of C QDs and CdTe QDs could be obtained at 405 nm (curve a) and 612 nm (curve b), respectively. As shown in the inset of Fig. 1D, the as-prepared C QDs solution is an almost transparent colorless liquid under visible light, while bright blue fluorescence is generated under the irradiation of a 365 nm UV lamp. CdTe QDs with strong red-emission fluorescence could also be observed under a 365 nm UV lamp. All these confirmed that blue-emission C QDs and red-emission CdTe QDs were successfully synthesized.

The surface functional groups of C QDs and CdTe QDs were characterized by FT-IR analysis (Fig. 2A). Curve a displayed the FT-IR spectrum of C QDs. Broad absorption at 3390 cm^{-1} from O–H/N–H stretching vibrations could be observed. The characteristic absorption bands at 2930, 1650 and 1055 cm^{-1} correspond to stretching vibrations of C–H, C=O and C–O/C–N stretching vibration, respectively. The peaks at 1573 cm^{-1} and 1404 cm^{-1} are assigned to –NH and C–N bonds. These confirmed the –OH, $–NH_2$ and –COOH bond on the surface of C QDs, the surface of the carbon quantum dots is grafted with rich oxygen-containing functional groups, such as hydroxyl and carboxyl groups, which proves its hydrophilic characteristics. Curve b indicated the FT-IR spectrum of CdTe QDs. The characteristic absorption peak of –OH stretching vibration of the carboxyl group could be observed at 3411 cm^{-1}. The symmetric and asymmetric vibrations of the –COO are located at 1394 and 1631 cm^{-1}, respectively.[47] Moreover, the characteristic absorption peak of –SH single bond stretching vibration of MPA at about 2567 cm^{-1} (curve c) could not be observed in the curve of CdTe QDs, indicating that the mercaptan group has been transformed into Cd–S coordination bond through covalent binding.[46] These confirmed the successful synthesis of –COOH modified CdTe QDs.

To construct the ratiometric fluorescent sensing platform, C QDs and CdTe QDs were combined for the dual-emission QDs solution. As shown in Fig. 2B, the pure C QDs were blue-emission with a single emission peak at 405 nm (curve a), and pure CdTe QDs were red-emission with a single emission peak at 612 nm (curve b). With the addition of CdTe QDs into C QDs, the fluoresce intensity at 612 nm increased while another at 405 nm decreased (curve c). To explore the reason for this, the concentration of the CdTe QDs added was further changed. As shown in Fig. 2C, the emission of C QDs gradually decreased with the increasing concentration of CdTe QDs, and the fluorescent color of the mixture changed from blue to purple, pink and red under 365 nm light irradiation. Moreover, the optical properties of the QDs were characterized. As seen from Fig. 2D, the absorption of CdTe QDs has a significant overlap with the emission of C QDs during the range from 365–550 nm, indicating that the fluorescence of C QDs might be quenched by CdTe QDs through Förster resonant energy transfer (FRET) with CdTe QDs as energy acceptors and C QDs as energy donors.[48,49]

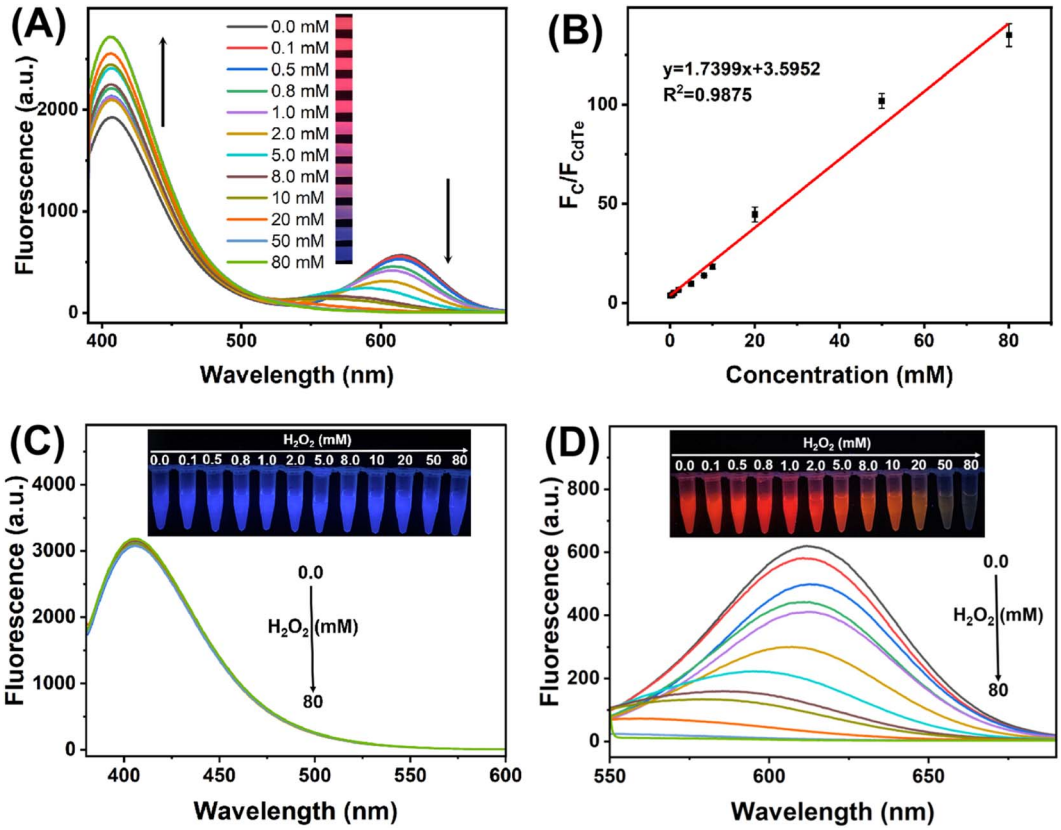

Fig. 3 (A) Fluorescence response of the mixed QDs to different concentrations of H_2O_2 from 0.0 to 80 mM. (B) Linear plot of the fluorescence intensity ratio (F_C/F_{CdTe}) against H_2O_2 concentration. Fluorescence responses of C QDs (C) and CdTe QDs (D) to different concentration of H_2O_2 from 0.0 to 80 mM. The insets show the photographs of corresponding solution under 365 nm UV light irradiation.

3.2 Feasibility study

The response of mixed QDs fluorescent system towards H_2O_2 was first studied in PBS (0.1 M, pH 7.0). As displayed in Fig. 3A, the fluorescence intensity of C QDs at 405 nm gradually recovered with the increased concentration of H_2O_2 from 0.0 to 80 mM, while the fluorescence intensity of CdTe QDs at 612 nm gradually quenched. In the meantime, the fluorescent color of the system changed from red to pink, purple and blue with the increasing H_2O_2 under 365 nm UV light irradiation. Moreover, there is a good linear relationship between the emission ratio of mixed QDs (F_C/F_{CdTe}) and the concentration of H_2O_2 within the range of 0.1–80 mM (R^2 = 0.9875) (Fig. 3B). Therefore, the ratiometric fluorescent sensing of H_2O_2 could be realized based on the mixed QDs strategy. Then, the response of pure QDs to

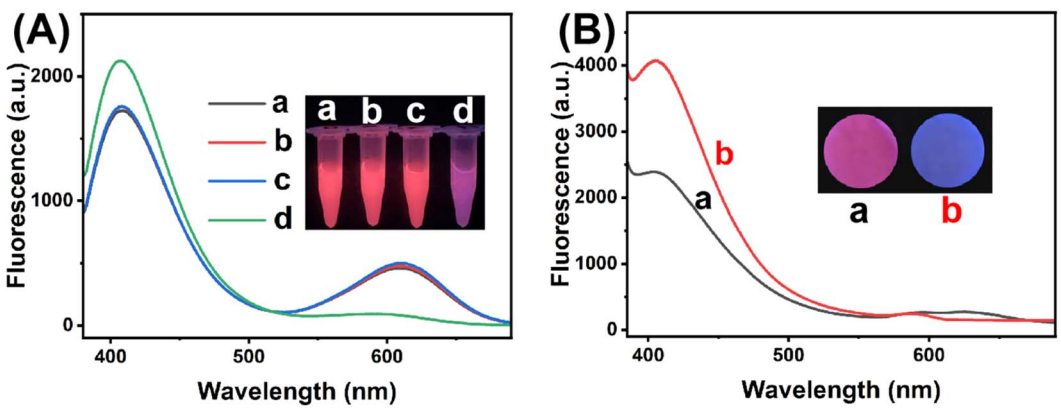

Fig. 4 (A) Fluorescence spectra of mixed QDs (a), mixed QDs + glucose (b), mixed QDs + GOx (c), and mixed QDs + glucose + GOx (d). (B) Fluorescence spectra of the paper-based ratiometric fluorescent sensing platform with (b) and without (a) glucose. The insets show the photographs of corresponding under 365 nm UV light irradiation.

H_2O_2 was further investigated. As seen from Fig. 3C, the addition of H_2O_2 had negligible effect on the fluorescence spectra of pure C QDs solution, and the blue fluorescence of C QDs remained nearly constant under 365 nm UV light irradiation. In contrast, the fluorescence intensity of CdTe QDs aqueous solution gradually decreased with the increase of H_2O_2 concentration from 0.0 to 80 mM (Fig. 3D), and the red fluorescence of CdTe QDs gradually faded with the increasing H_2O_2 under 365 nm UV light irradiation. These results indicated that the ratiometric fluorescence signals of mixed QDs could be obtained by quenching the fluorescence of CdTe QDs with H_2O_2.

To further explore the feasibility of mixed QDs system for glucose detection, control experiments have been carried out. As seen from Fig. 4A, both glucose and glucose oxidase (GOx) exhibited negligible influences on the fluorescence spectra of mixed QDs solution. When glucose and GOx coexisted in the mixed QDs system, the fluorescence spectra changed obviously, and the fluorescent color changed from red to pink under 365 nm UV light irradiation, which is consistent with the effect of H_2O_2. The reason might be that GOx catalyzed glucose oxidation to produce gluconic acid and H_2O_2, and the latter quenched the fluorescence of CdTe QDs, leading to the recovery of C QDs emission. Moreover, the feasibility of glucose detection by the paper-based sensing platform was also investigated (Fig. 4B). In the absence of glucose, the paper-based sensing platform with pink fluorescent color under 365 nm UV light irradiation displayed the fluorescence of C QDs and CdTe QDs simultaneously. With the introduction of glucose, the fluorescence of CdTe QDs decreased while the fluorescence of C QDs increased, and a noticeable fluorescent color change from pink to blue could be observed. These results verified that the paper-based ratiometric fluorescent sensing platform based on the mixed QDs strategy could be successfully fabricated and applied for glucose detection.

3.3 Optimization of experimental conditions

In order to achieve maximal color change in the paper-based ratiometric fluorescent sensing platform, the blue-to-red emission ratio must be optimized, as the range of color change is dependent on the fluorescence intensity ratio of the two materials. Thus, the composition ratio of the mixed QDs system was firstly optimized by gradually changing the concentration of CdTe QDs in the mixed QDs system while keeping the amount of C QDs constant. As seen from Fig. 5A, with the increasing concentration of CdTe QDs in the mixed QDs system, the fluorescent color of the paper-based sensing platform changed from blue to purple, pink and red under 365 nm UV light irradiation, and the emission ratio of mixed QDs (F_C/F_{CdTe}) decreased gradually. It is worth noting that further increasing the CdTe QDs concentration after 1 mg mL^{-1} caused little change in the value of F_C/F_{CdTe}. Thus, the optimal concentration of CdTe QDs applied in the mixed QDs system was chosen at 1 mg mL^{-1}.

Considering that the ratiometric fluorescence signal of the paper-based sensing platform towards target glucose relies on the H_2O_2 produced from the catalytic oxidation process by GOx, the amount of GOx was also optimized by changing the concentration of GOx applied during the fabrication process. As shown in Fig. 5B, the value of F_C/F_{CdTe} initially increased with increasing GOx concentration and reached a plateau after 40 U mL^{-1}. Accordingly, the optimal concentration of GOx applied in the paper-based sensing platform fabrication was selected as 40 U mL^{-1}.

Catalytic reaction time is another critical factor that affects the performance of the paper-based sensing platform for glucose detection. The relationship between reaction time and the value of F_C/F_{CdTe} has been displayed in Fig. 5C. It could be seen that the value of F_C/F_{CdTe} increased with the increase of reaction time and tended to level off after 50 min. In order to save time during the experiment, it was determined that 50 minutes would be the optimal reaction time.

3.4 Performance of the paper-based sensing platform

Under optimized experimental conditions, fluorescence spectra were measured for the paper-based ratiometric fluorescent sensing platforms with varying glucose concentrations. As displayed in Fig. 6A, emission peaks of C QDs and CdTe QDs exhibited different variation trends with glucose concentration. The emission of CdTe QDs was gradually quenched with the increasing concentration of glucose, while the emission of C QDs was gradually enhanced with that. In the meantime, the fluorescent color of the paper-based sensing platform changed with the increasing glucose concentration from pink to purple

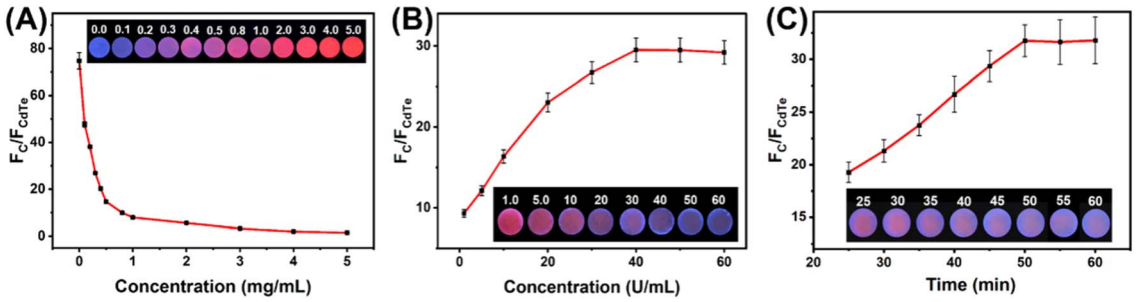

Fig. 5 (A) Effects of CdTe QDs concentration on the fluorescence intensity ratio (F_C/F_{CdTe}) of the mixed QDs system. Effects of the GOx concentration (B) and reaction time (C) on the fluorescence responses of the paper-based fluorescent sensors. The insets are the corresponding photographs under a 365 nm UV lamp.

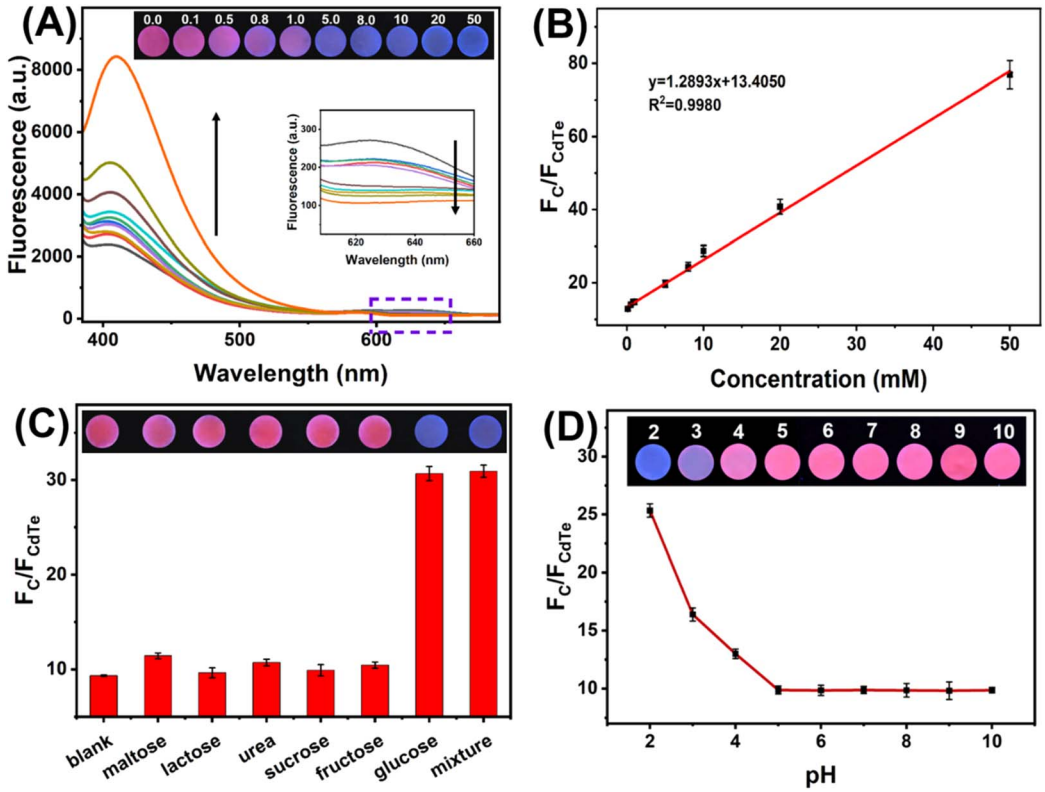

Fig. 6 (A) Fluorescence spectra of the paper-based sensors with the addition of glucose with different concentrations. (B) Linear plot of the fluorescence intensity ratio (F_C/F_{CdTe}) against glucose concentration (0.1 mM to 50 mM). (C) Selectivity of the paper-based ratiometric fluorescent sensing platform. (D) The response of the paper-based sensing platform to different pH conditions. The insets are the corresponding photographs under 365 nm UV light irradiation.

and blue. Moreover, a linear relationship could be obtained between the value of F_C/F_{CdTe} and glucose concentration during the range from 0.1 mM to 50 mM (Fig. 6B). The linear calibration curve was calculated and fitted as $y = 1.2893x + 13.4050$ ($R^2 = 0.9980$) (y refers to the value of F_C/F_{CdTe}, while x refers to the concentration of glucose). The limit of detection based on $3\sigma/k$ was 0.026 mM, where σ is the standard deviation of the blank ($n = 3$) and k is the slope of the linear calibration curve.

The selectivity of the paper-based sensing platform towards glucose was also investigated. As shown in Fig. 6C, the signal responses of the paper-based sensors to maltose, lactose, urea, sucrose, and fructose were comparable with blank, indicating that these substances had negligible effects on the fluorescence signal of the paper-based sensing platform. By contrast, about 3-fold enhanced signal response could be obtained when glucose with the same concentration (10 mM) was present. In addition, the influence of interfering substances on glucose detection was also explored. It could be seen that both the value of F_C/F_{CdTe} and the fluorescent color under 365 nm UV light irradiation changed little with the introduction of interfering substances during glucose detection. These results indicate that the fabricated paper-based ratiometric fluorescent sensing platform has good selectivity and anti-interference ability for glucose.

The stability of the fabricated paper-based ratiometric fluorescent sensing platform was further studied by monitoring the value of F_C/F_{CdTe} over 40 days. The QDs-GOx-impregnated paper was stored in a refrigerator at 4 °C and measured intermittently. The value of F_C/F_{CdTe} barely changed after 9 days of storage and kept 91.2% of the initial signal after storage for 40 days. Additionally, the reproducibility of the paper-based ratiometric fluorescent sensing platform was estimated by conducting the inter-assay and intra-assay with 10 mM glucose. The ratiometric signal responses of paper-based fluorescent sensors were recorded in one batch and different batches, respectively. The relative standard deviation (RSD) of the inter-assay and intra-assay were 2.26% and 4.70%, respectively. These results reveal that the fabricated paper-based ratiometric fluorescent sensing platform possesses good stability and reproducibility.

In addition, the response of the paper-based ratiometric fluorescent sensing platform to different pH conditions was also investigated. As shown in Fig. 6D, the value of F_C/F_{CdTe} remains unchanged during the pH range of 5–10. When the pH comes to lower than 5, the value of F_C/F_{CdTe} increases with the decrease of pH. Considering the effects of pH conditions and the pH of the actual urine sample (near neutral), PBS (0.1 M, pH 7.0) was chosen to adjust the pH value for real sample testing.

3.5 Detection of glucose in urine samples

Recovery tests were conducted to verify the practicability of fabricated paper-based sensors for urine glucose detection.

Table 1 Determination of glucose spiked in the urine samples using the proposed method ($n = 3$)

Sample		Added (mM)	Visual analysis: Photograph	Found detected: Concentration (mM)	Recovery (%)	RSD (%)
Volunteer 1	0	0.00		—	—	—
	1	0.500		0.497	99.4	2.35
	2	5.00		5.01	100	3.23
	3	10.0		9.63	96.3	0.587
Volunteer 2	0	0.00		—	—	—
	1	0.500		0.468	93.6	3.34
	2	5.00		4.74	94.8	4.26
	3	10.0		10.1	101	3.85
Volunteer 3	0	0.00		—	—	—
	1	0.500		0.52	104	3.47
	2	5.00		4.79	95.8	8.72
	3	10.0		10.2	102	3.61

Before measurement, urine samples were diluted with an equal volume of PBS (0.1 M, pH 7.0) and spiked with different concentrations of glucose. As shown in Table 1, the recoveries of samples in three spiked levels were calculated to be 93.6–104%, with RSD ranging from 0.587% to 8.72%. Thus, the paper-based ratiometric fluorescent sensing platform processes good anti-interference capabilities for practical applications.

4. Conclusion

In summary, a ratiometric fluorescent sensing system with signal response to glucose has been reasonably designed based on the interaction between CdTe QDs and C QDs, as well as the quenching effect of H_2O_2 on CdTe QDs. The paper-based sensing platform for urine glucose has been successfully constructed by simply immobilizing mixed QDs and GOx on paper. The simultaneous excitation of C QDs and CdTe QDs could be achieved using portable 365 nm UV light. The intensity of two kinds of QDs changed with the increasing glucose concentration, and the resulting fluorescent color change can be easily distinguished by the naked eye. Moreover, the paper-based ratiometric fluorescent sensing platform with satisfactory selectivity, good stability and excellent reproducibility can be easily fabricated at low cost and provide a simple and portable platform for glucose analysis.

Author contributions

Keke Song: methodology, data curation, writing – original draft. Chenying Liu: investigation, validation. Guangbin Chen: data curation. Wenhao Zhao: data curation. Shufang Tian: writing – review & editing. Qian Zhou: conceptualization, funding acquisition, supervision.

Conflicts of interest

The authors have no conflict to declare.

Acknowledgements

This work was supported by the National Natural Science Foundation of China (22004027), the China Postdoctoral

Science Foundation (2020M682275), the Science and Technology Research Project of Henan Province (202102310466).

References

1 X. Jiang, C. Sun, Y. Guo, G. Nie and L. Xu, *Biosens. Bioelectron.*, 2015, **64**, 165–170.
2 A. L. Galant, R. C. Kaufman and J. D. Wilson, *Food Chem.*, 2015, **188**, 149–160.
3 A. Pandey, P. Tripathi, R. Pandey, R. Srivatava and S. Goswami, *J. Pharm. BioAllied Sci.*, 2011, **3**, 504–512.
4 H. H. Do, S. Y. Kin and Q. V. Le, *Microchem. J.*, 2023, **193**, 10920.
5 T. Koschinsky and L. Heinemann, *Res. Rev.*, 2001, **17**, 113–123.
6 Y. Yao, J. Chen, Y. Guo, T. Lv, Z. Chen, N. Li, S. Cao, B. Chen and T. Chen, *Biosens. Bioelectron.*, 2021, **179**, 113078.
7 S. Patra, S. S. Purohit and S. K. Swain, *Microchem. J.*, 2023, **190**, 108646.
8 C. J. Bailey and P. J. Grant, *Lancet*, 1998, **352**, 1932.
9 Q. Dong, H. Ryu and Y. Lei, *Electrochim. Acta*, 2021, **370**, 137744.
10 T. Zhao, Y. Li, X. Zhang, H. Lyu and Z. Xie, *Microchem. J.*, 2023, **186**, 108363.
11 F. Zamboni and M. N. Collins, *Int. J. Pharm.*, 2017, **521**, 346–356.
12 A. Beaucamp, M. Culebrasa and M. N. Collins, *Green Chem.*, 2021, **23**, 5696–5705.
13 J. Park, J. Kim, S. Kim, W. H. Cheong, J. Jang, Y. Park, K. Na, Y. Kim, J. H. Heo, C. Y. Lee, J. H. Lee, F. Bein and J. Park, *Sci. Adv.*, 2018, **4**, 9841.
14 C. Liu, C. Liu, Y. Lai, C. Lee, S. Gupta and N. Tai, *Microchem. J.*, 2023, **191**, 108872.
15 B. Saini and T. K. Mukherjee, *ACS Appl. Mater. Interfaces*, 2022, **14**, 53462–53474.
16 P. Lin, S. Sheu, C. Chen, S. Huang and B. Li, *Talanta*, 2022, **241**, 123187.
17 M. N. Karim, S. R. Anderson, S. Singh, R. Ramanathan and V. Bansal, *Biosens. Bioelectron.*, 2018, **110**, 8–15.
18 T. Lee, I. Kim, D. Y. Cheong, S. Roh, H. G. Jung, S. W. Lee, H. S. Kim, D. S. Yoon, Y. Hong and G. Lee, *Anal. Chim. Acta*, 2021, **1158**, 338387.
19 L. R. Morris, J. A. McGee and A. E. Kitabchi, *Ann. Intern. Med.*, 1981, **94**, 469–471.
20 S. Liu, Z. Shen, L. Deng and G. Liu, *Biosens. Bioelectron.*, 2022, **209**, 114251.
21 W. Dong, G. Chen, M. Ding, H. Cao, G. Li, M. Fang and W. Shi, *Microchem. J.*, 2023, **188**, 108448.
22 P. Dang, X. Liu, H. Ju and J. Wu, *Anal. Chem.*, 2020, **92**, 5517–5523.
23 H. Sun, J. Zhang, M. Wang and X. Su, *Microchem. J.*, 2022, **179**, 107574.
24 S. Hu, Y. Jiang, Y. Wu, X. Guo, Y. Ying, Y. Wen and H. Yang, *ACS Appl. Mater. Interfaces*, 2020, **12**, 55324–55330.
25 Z. Yang, S. Chen, Y. Zhao, P. Zhou and Z. Cheng, *Sens. Actuators, B*, 2018, **266**, 422–428.
26 Y. Li, Y. Deng, X. Zhou and J. Hu, *Talanta*, 2018, **179**, 742–752.
27 J. Shen, Z. Wang, D. Sun, C. Xia, S. Yuan, P. Sun and X. Xin, *ACS Appl. Mater. Interfaces*, 2018, **10**, 3955–3963.
28 J. Yang, Z. Li and Q. Jia, *Sens. Actuators, B*, 2019, **297**, 126807.
29 X. Guo, D. Xu, H. Yuan, Q. Luo, S. Tang, L. Liu and Y. Wu, *J. Mater. Chem. A*, 2019, **7**, 27081–27088.
30 J. Zhou, B. Li, A. Qi, Y. Shi, J. Qi, H. Xu and L. Chen, *Sens. Actuators, B*, 2020, **305**, 127462.
31 Y. Zhang, D. Hou, Z. Wang, N. Cai and C. Au, *Polymers*, 2021, **13**, 2540.
32 B. Shi, X. Zhang, W. Li, N. Liang, X. Hu, J. Xiao, D. Wang, X. Zou and J. Shi, *Food Chem.*, 2023, **400**, 133995.
33 A. Bigdeli, F. Ghasemi, S. Abbasi-Moayed, M. Shahrajabian, N. Fahimi-Kashani, S. Jafarinejad, M. A. F. Nejad and M. R. Hormozi-Nezhad, *Anal. Chim. Acta*, 2019, **1079**, 30–58.
34 Y. Shu, Q. Ye, T. Dai, J. Guan, Z. Ji, Q. Xu and X. Hu, *J. Hazard. Mater.*, 2022, **430**, 128360.
35 L. Zong, Y. Jiao, X. Guo, C. Zhu, L. Gao, Y. Han, L. Li, C. Zhang, Z. Liu, J. Liu, Q. Ju, H. Yu and W. Huang, *Talanta*, 2019, **195**, 333–338.
36 Y. Lin, S. Ye, J. Tian, A. Leng, Y. Deng, J. Zhang and C. Zheng, *J. Hazard. Mater.*, 2023, **459**, 132201.
37 B. Li, Z. Zhang, J. Qi, N. Zhou, S. Qin, J. Choo and L. Chen, *ACS Sens.*, 2017, **2**, 243–250.
38 Z. Sheng, H. Han, X. Hu and C. Chi, *Dalton Trans.*, 2010, **39**, 7017–7020.
39 L. Zou, Z. Gu, N. Zhang, Y. Zhang, Z. Fang, W. Zhu and X. Zhong, *J. Mater. Chem.*, 2008, **18**, 2807–2815.
40 M. Zhou, Z. Zhou, A. Gong, Y. Zhang and Q. Li, *Talanta*, 2015, **143**, 107–113.
41 Z. Qiu, J. Shu and D. Tang, *Anal. Chem.*, 2017, **89**, 5152–5160.
42 A. N. Emam, S. A. Loutfy, A. A. Mostafa, H. Awad and M. B. Mohamed, *RSC Adv.*, 2017, **7**, 23502–23514.
43 B. Kong, A. Zhu, C. Ding, X. Zhao, B. Li and Y. Tian, *Adv. Mater.*, 2012, **24**, 5844–5848.
44 S. Zhu, Q. Meng, L. Wang, J. Zhang, Y. Song, H. Jin, K. Zhang, H. Sun, H. Wang and B. Yang, *Angew. Chem., Int. Ed.*, 2013, **52**, 3953–3957.
45 Y. Lin, Q. Zhou, D. Tang, R. Niessner, H. Yang and D. Knopp, *Anal. Chem.*, 2016, **88**, 7858–7866.
46 T. Liu, L. Fu, C. Yin, M. Wu, L. Chen and N. Niu, *Microchem. J.*, 2022, **174**, 107016.
47 S. Lu, Z. Li, X. Fu, Z. Xie and M. Zheng, *Dyes Pigm.*, 2021, **187**, 109126.
48 Q. Zhu, J. Du, S. Feng, J. Li, R. Yang and L. Qu, *Spectrochim. Acta, Part A*, 2022, **267**, 120492.
49 J. Hottechamps, T. Noblet, C. Méthivier, S. Boujday and L. Dreesen, *Nanoscale*, 2023, **15**, 2614–2623.